DE GRUYTER

Chemical Papers 70 (11) 1503–1511 (2016)
DOI: 10.1515/chempap-2016-0084

ORIGINAL PAPER

Identification of selective oxidation of TiC/SiC composite with X-ray diffraction and Raman spectroscopy

[a,b]Nicoleta Doriana Banu, [a,c]Ionut Banu*, [a]Marios S. Katsiotis, [a]Anjana Tharalekshmy, [a]Samuel Stephen, [a,d]Jamie Whelan, [a]Gisha Elizabeth Luckachan, [a]Radu Vladea, [a]Saeed M. Alhassan

[a] *Department of Chemical Engineering, The Petroleum Institute, P.O. Box 2533, Abu Dhabi, United Arab Emirates*

[b] *Centre for Organic Chemistry "C.D. Nenitescu", Romanian Academy, Spl. Independentei 202B, 060023, Bucharest, Romania*

[c] *Department of Chemical and Biochemical Engineering, University Politehnica of Bucharest, 313 Spl. Independentei, sector 6, 060042, Bucharest, Romania*

[d] *Department of Chemistry, New York University Abu Dhabi, P.O. Box 129188, Abu Dhabi, United Arab Emirates*

Received 5 December 2015; Revised 1 March 2016; Accepted 24 March 2016

Open cell 3D titanium carbide/silicon carbide (TiC/SiC) composite was oxidised to titanium oxide/silicon carbide (TiO_2/SiC) following different temperature profiles in a thermal gravimetric analysis (TGA) instrument in continuous air-flow and static air (oven) environments. The TiC oxidation to anatase, starting at temperatures over 450 °C, was confirmed by Raman spectroscopy and X-Ray diffraction (XRD). By increasing the temperature, the mass fraction of anatase diminished, while the mass fraction of rutile increased. SiC oxidation started at 650 °C when a mixture of TiO_2/SiO_2/SiC could be observed by Raman, XRD and HRTEM.

Keywords: selective oxidation, TiC/SiC composite, X-ray diffraction, Raman spectroscopy, anatase, rutile

Introduction

Due to their suitable physical properties such as their low density, high surface area and pore volume, high thermal and chemical stability (Xia et al., 2013), carbide materials have been widely used as catalyst supports in recent studies (Nguyen & Pham, 2011; Schmirler et al., 2011). Among the carbides used for catalysis, silicon carbide (SiC) is known to have high chemical inertness and high thermal conductivity (Li et al., 2007), rendering it suitable for various applications including: electronic and optical devices (Li et al., 2007), high temperature sensors (Li et al., 2007; Nguyen & Pham, 2011), selective oxidation of H_2S (Nguyen & Pham, 2011) and enhanced steam-reforming process (Basile et al., 2007; Wang et al., 2008). The versatility of SiC means that it can be synthesised in a variety of shapes and with differing surface areas (Nguyen et al., 2009; de Tymowski et al., 2012).

Titanium carbide (TiC) is another carbon-based material widely used in industry due to its extreme hardness and wear-resistance properties (Fernandez-Torres et al., 2002). This carbide can be readily transformed to titanium oxide (TiO_2) by simple thermal oxidation starting at 350 °C (Zhang & Koka, 1998); the synthesis, properties and applications of TiO_2 have already been extensively discussed elsewhere (Diebold, 2003; Long et al., 2008; Moene et al., 1998; Mirabedini et al., 2011; Nguyen & Pham, 2011). The oxidation of TiC to TiO_2 is a multi-step exothermic process consisting of four consecutive reaction steps: TiC →

*Corresponding author, e-mail: i_banu@chim.upb.ro

oxycarbide (TiC_xO_{1-x}) → suboxides such as TiO, Ti_3O_5 or Ti_4O_9 → anatase → rutile (TiO_2) (Shimada, 1996; Zhang & Koka, 1998). TiO_2 exists in three polymorphs: rutile (tetragonal), anatase (tetragonal) and brookite (orthorhombic) (Okada et al., 2001; Hu et al., 2003), but the anatase transition to rutile is the most frequently discussed given that anatase is a valuable dielectric material used in photocatalysis (Okada et al., 2001; Savio et al., 2012) and solar cells (Nguyen et al., 2007) while rutile is widely used in Earth Sciences (Meinhold, 2010) and photocatalysis (Long et al., 2008). Anatase transformation to rutile can be influenced by several parameters including temperature, sample geometry and purity (Moene et al., 1998; Hu et al., 2003; van der Meulen et al., 2007; Savio et al., 2012).

Recent studies in the literature have reported a new way of producing open cell 3D TiC/SiC composites with high specific surface area (Nguyen & Pham, 2011). Since several of the catalytic processes which use TiO_2 operate at high temperatures (e.g. steam methane- reforming (Basile et al., 2007)) and under oxidative environments (volatile organic compounds catalytic combustion (Marin et al., 2012)), and knowing that SiC reacts with oxygen at around 750 ℃ (Basile et al., 2007), understanding this new composite material's behaviour under oxidative conditions becomes an important issue. It is expected that the presence of SiC in the open cell 3D TiC/SiC composite has an influence on TiC oxidation to TiO_2, hence, from a physicochemical perspective, it is useful to know the oxidation behaviour of such new open cell composites. The current study presents a detailed analytical characterisation of a thermally induced TiC/SiC oxidation to TiO_2/SiC following different oxidation temperatures with an emphasis on anatase to rutile transformation.

Experimental

TiC/SiC 3D open cell composite (SICAT Germany) was oxidised in static air in an oven at different temperatures (℃): 350, 450, 550, 650 and 750; the temperature was increased with a heating rate of 3 ℃ min^{-1} and then maintained for 3 h. After oxidation, the sample was cooled to ambient temperature and then analysed using several techniques. The samples were denoted as follows: oxtemperature (example given Ox350).

Characterisation of TiC/SiC composite oxidation

Thermal gravimetric analysis (TGA-DTA, LINSEIS STA PT1600 system) coupled with a mass spectrometer (MS, Pfeiffer) was used in the present study to determine the raw composite behaviour during oxidative treatment from ambient temperature up to 800 ℃. The measurement was perforrtmed with a heating rate of 3 ℃ min^{-1}, under a dynamic air atmosphere (a flow-rate of 50 mL min^{-1}). The composite was cut into small pieces preserving the 3D cell shape and placed in alumina crucibles.

X-ray diffraction (XRD) patterns were collected using a Panalytical Powder diffractometer (X'Pert PRO). The powder samples were prepared on a Zero Background Holder and were mounted on the diffractometer using the reflection – transmission stage. All samples were measured in Bragg–Brentano geometry. The power settings for the CuK_α radiation were 45 kV and 40 mA. The detector used was an X'Celerator from Panalytical and the experiment was performed in reflection mode using Gonio geometry.

The materials were characterised in the solid-state by FT-IR spectroscopy using a Bruker VERTEX 70 instrument equipped with a Miracle zirconium ATR device, collecting 32 scans in the range 500–4000 cm^{-1}.

Surface chemical modification of the 3D TiC/SiC composite during oxidation was characterised by Raman spectroscopy (Horiba JobinYvon instrument) using a green laser (λ = 514 nm) and the 50× objective lens.

For Scanning Electron Microscope (SEM) sample preparation, a small amount of powder was used (≈ 20 μg) of each specimen. The samples were set on standard SEM sample holders (stubs) using conductive silver glue and the analyses were conducted on a FEI Quanta 250 (FEG) SEM, coupled with an energy dispersive X-ray analysis (EDX). In order to ensure statistical repeatability and obtain a clear depiction of the structure, shape and size of the TiC/SiC composite, a minimum of 10 images of every sample were collected at each magnification.

High Resolution Transmission Electron Microscopy (HRTEM) was performed using a FEI Tecnai G20 with a 0.11 nm point-to-point resolution, operated at 200 kV. The microscope was coupled with an EDS X-ray analyser, making possible the determination of elemental composition. In addition, elemental mapping was performed using Energy Filtered TEM (EFTEM) with a post column energy filtered camera (Gatan GIF 963), having an energy resolution better than 0.85 eV (FWHM at the zero loss peak). The "three-window" method (Worch et al., 2002) was applied to acquire the maps. With regard to sample preparation, initially powder samples were ground for 15 min in a mortar. Next, approximately 3 mg of each sample was mixed with 30 mL of high purity ethanol (99.99 %). Each mixture was treated in an ultrasonic bath for 5 min at ambient temperature and two drops of each suspension were deposited on 300 mesh (0.053 mm) copper grids covered with thin amorphous carbon film (lacey carbon). For a typical experiment, the sample was inserted immediately following preparation, to avoid contamination. EDS was used

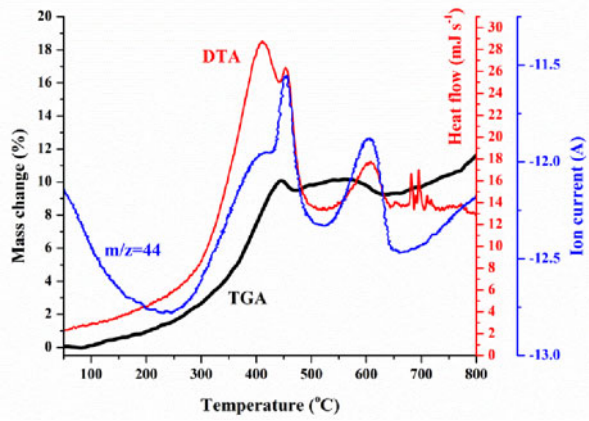

Fig. 1. Simultaneous TGA-DTA-MS analysis for TiC/SiC in dynamic air flow.

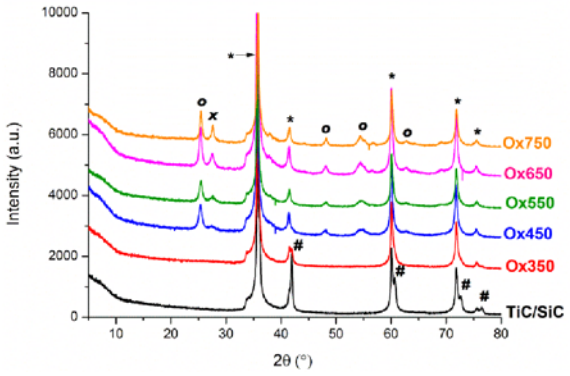

Fig. 2. XRD patterns of raw and oxidised TiC/SiC: SiC (∗), TiC (#), rutile (×), anatase (○).

to define the elemental composition. EFTEM mapping was performed on several areas of low thickness (< 150 nm) and the samples were found to be chemically homogeneous at the probe scale (≈ 90 nm).

Results and discussion

Thermal gravimetric analysis coupled with mass spectrometry

Oxidation of TiC leads to a change in the sample colour at temperatures higher than 450 ℃ as observed by visual inspection; the initial sample colour is dark grey and becomes light grey after oxidation.

TGA-DTA-MS was used in the present study to assess the sample's thermal stability in a dynamic oxidative environment (air), with Fig. 1 showing the thermal behaviour of the TiC/SiC material under non-isothermal conditions in the temperature range of 50–850 ℃. A mass gain can be seen in TGA due to material oxidation (Ghanem et al., 2007), presented as mass change (%) on the axis.

Due to continuous phase modification during TiC oxidation to TiO_2, the mass change steps overlap, hence cannot be separated and individually evaluated. Accordingly, a simultaneous TGA-DTA instrument served to evaluate the mass change steps by matching the corresponding oxidative behaviour in DTA with the mass gain in TGA. Two exothermic peaks can be observed in DTA at 411 ℃ and 453 ℃, corresponding to two overlapping mass evolution steps in TGA and are due to the formation of oxycarbide and anatase (Shimada, 1996; Zhang & Koka, 1998). The third step has a maximum at 608 ℃ and can be attributed to rutile generation while the small oxidation peaks above 650 ℃ are due to SiC oxidation to SiO_2. The literature recognises that the reaction of TiC with oxygen leads to TiO_2 and CO_2 (Shimada, 1996). Fig. 1 also shows the evolution of mass fragment $m/z = 44$ (CO_2). It can be observed that the CO_2 evolution followed the same pattern with the first three exothermic peaks in DTA (℃): 411, 453 and 608, characteristic of TiC oxidation. Considering these results, the decision was made to oxidise the TiC/SiC material at different temperatures (℃): 350, 450, 550, 650 and 750, keeping the set-point temperature value constant for 3 hours in order to oxidise the TiC/SiC composite to TiO_2/SiC.

X-ray diffraction

XRD patterns were collected for the structural characterisation of the sample treated at different temperatures (Fig. 2).

The XRD pattern for the raw material shows the characteristic peaks for both SiC, 2θ (°): 35.8, 41.5, 60.1, 71.8 and 75.6 and for TiC 41.9, 60.6, 72.6 and 76.4. The TiC structure modification can be observed in XRD starting with Ox350. The crystalline structures of TiO_2, i.e. rutile and anatase, both tetragonal (Ohsaka et al., 1979), are visible in the XRD patterns from Ox450 to Ox750. Anatase shows five peaks, 2θ (°): 25.4, 37.9, 48.2, 55.2 and 62.8, while rutile has two at 27.6 and 56.7. The XRD pattern of the oxidised samples shows two peaks characteristic of tetragonal TiO_2, 2θ (°): 54.4 and 69.1. Since the XRD peaks for TiO_2 are different, an assumption can be made about the mass fraction between these two oxides by calculating the ratio between the anatase and rutile phases (Eq. (1) (Hu et al., 2003; Sreekantan et al., 2009)). This calculation takes into account the (101) anatase peak ($2\theta = 25.4°$) and (110) rutile ($2\theta = 27.6°$):

$$X_A = \left(1 + 1.26\frac{I_R}{I_A}\right)^{-1} \quad (1)$$

where X_A is the relative mass factor of anatase, I_A and I_R are the XRD integrated intensities of (101) anatase and (110) rutile. A decrease in the anatase phase content with the increasing oxidation temperature can be observed (X_A is 0.70 for Ox550, 0.66 for Ox650 and 0.62 for Ox750). This observation is in agreement with the Raman spectroscopy results.

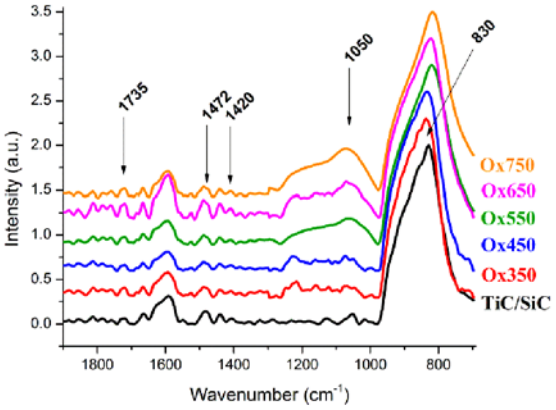

Fig. 3. FT-IR spectra of raw and oxidised composite.

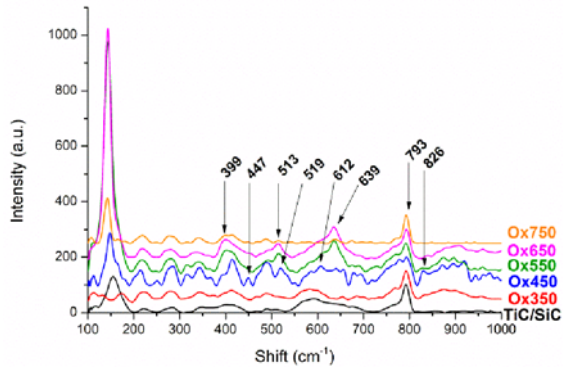

Fig. 4. Raman spectra of raw and oxidised TiC/SiC, region between 100–1000 cm^{-1}.

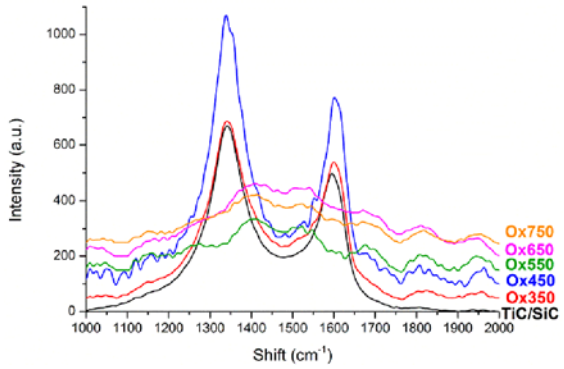

Fig. 5. Raman spectra of raw and oxidised TiC/SiC between 1000–2000 cm^{-1}.

Solid-state by FT-IR spectroscopy

The FT-IR ATR technique was used in the present study for characterisation of the material surface after different oxidation temperatures. Both SiO_2 and TiO_2 exhibit peaks in the wavelength range of 700–1800 cm^{-1}. Fig. 3 shows the FT-IR spectra for raw and oxidised samples, all plots being normalised in respect to the highest peak at 800 cm^{-1}.

Both SiO_2 and SiC display characteristic peaks in the 800–1200 cm^{-1} region (Duran et al., 1986; Raman et al., 2006; Mirabedinia et al., 2011). The peak at around 840 cm^{-1} (shoulder at 950 cm^{-1}) can be attributed to Si—C linkage (Merlemejean et al., 1995; Raman et al., 2006), while the absorption band at 1100 cm^{-1} corresponds to silica (Merlemejean et al., 1995). The raw TiC/SiC composite main peak is the Si—C linkage at 830 cm^{-1} with a small shoulder in the 950 cm^{-1} region confirming the presence of SiC and the absence of oxide in the initial material (Merlemejean et al., 1995).

The characteristic peak for silica (Duran et al., 1986; Merlemejean et al., 1995) is located at 1100 cm^{-1} while titanium oxides exhibit peaks (cm^{-1}): 1735, 1472, 1420, 1150 and 1106 (anatase) (Moene et al., 1997). It should be noted that both TiO_2 and SiO_2 present peaks in the region between 1000 cm^{-1} and 1200 cm^{-1}, but the fact that these two peaks overlap renders the correct attribution only by IR in this region a difficult task.

The small shift of the SiC peak from 830 cm^{-1} to 818 cm^{-1} for Ox750 can be due to the presence of SiO_2, indicating that the SiC structure is no longer intact at this temperature.

Raman spectroscopy

In comparison with IR, Raman spectroscopy gives more information on the type of TiO_2 (rutile or anatase) formed during the oxidation process (Fig. 4). The spectra are normalised (Si—C peak at 793 cm^{-1}) and the curves are fitted using the Gaussian–Lorentzian function.

For the raw and thermally treated samples at temperatures up to 650 °C, the presence of the Si—C peak at 793 cm^{-1} (Raman et al., 2006; Li et al., 2007) and the absence of silica peaks (cm^{-1}): 460, 810 and 1065 (Yoshikawa et al., 1997) were observed. Raman spectra for Ox750 show the presence of silica in the oxidised material, in agreement with FT-IR analysis and with the data in the literature (Moene et al., 1998; Nguyen & Pham, 2011).

Anatase has six active modes in Raman (A1g + 2B1 + 3Eg) while rutile has four active modes (A1g + B1g + B2g + Eg) (Ohsaka et al., 1979; Orendorz et al., 2007). The Raman spectrum of anatase shows peaks (cm^{-1}): 144, 197, 399, 513, 519 and 639, while the spectrum of rutile shows peaks: 143, 447, 612 and 826. Anatase formation can be observed in the Raman spectra (Fig. 5) up to 550 °C; beyond this temperature TiO is present in rutile form. The Raman spectra show that rutile is the major phase for Ox750, an observation in agreement with XRD results and the data in the literature (Sreekantan et al., 2009).

The characteristic Raman peaks for carbon, namely the D and G bands, are present in carbides (Schwan et al., 1996). The presence of the D and G bands can be observed for TiC/SiC and for the composite ox-

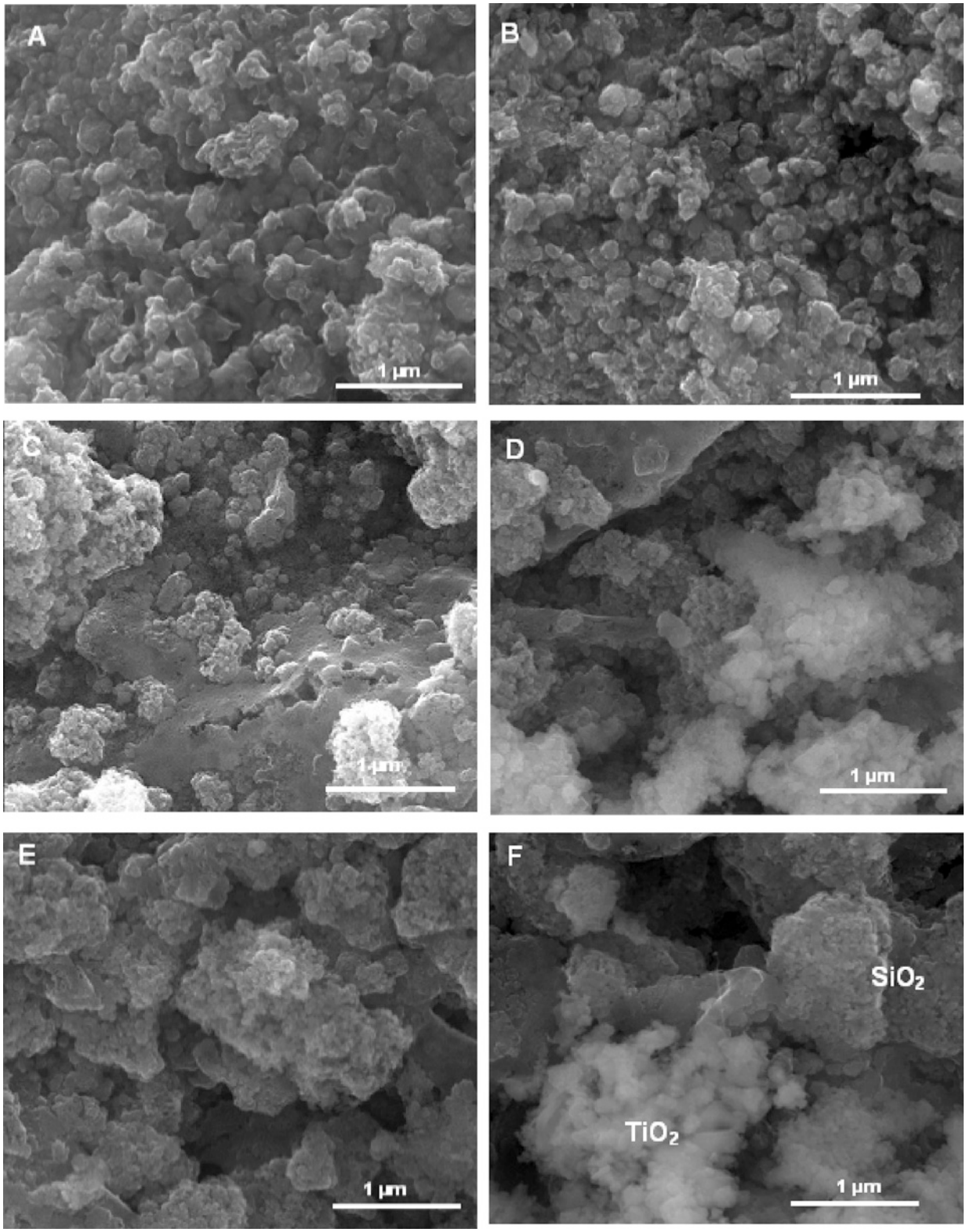

Fig. 6. SEM images of raw (A), Ox350 (B), Ox450 (C), Ox550 (D), Ox650 (E) and Ox750 (F).

idised at low temperatures (up to 450 °C). For temperature values over 550 °C, a decrease in intensity for the D and G peaks can be observed from Fig. 5. This modification is mainly due to the amorphous carbon consumption.

SEM and HRTEM

SEM images (Fig. 6) show the phase difference between TiC and SiC in the raw composite. Nguyen and Pham (2011) show a well-dispersed TiC on the SiC for

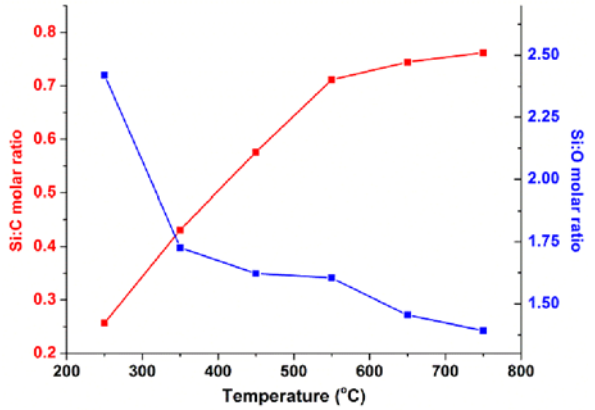

Fig. 7. Progression of Si:C and Si:O with temperature.

the same composite. After oxidation, a phase modification can be observed due to TiO_2 formation (rutile and anatase), confirmed by XRD (Fig. 2) and TEM (Fig. 7) below. The presence of SiO_2 at 750 ℃ is further confirmed by the SEM results. The lack of SiO_2 peaks in the XRD can be attributed to the tendency of SiO_2 to remain amorphous at a high temperature and pressure (Martoňák et al., 2006).

SEM analysis of the as-received sample shows a homogeneous morphology of the inner structure and an excellent dispersion of TiC on SiC. Specifically, the TiC particles range in size from 40 nm to 200 nm and appear to be embedded in the SiC structure.

Regarding the thermally treated samples, EDX analysis shows the oxygen concentration as increasing with the oxidation temperature, attaining a maximum of 28 % (average) at 750 ℃. In addition, the structure becomes less homogeneous in size due to the formation of TiO_2 particles.

The progression of Si/C and Si/O with temperature (Fig. 7) shows a decrease in the Si/C ratio and an increase in the Si/O ratio, possibly due to SiC oxidation.

The TEM micrographs (Fig. 8) and mapping (Fig. 9) of the TiC/SiC composite show the TiC particles embedded in the SiC matrix, in agreement with the SEM analyses (Fig. 6).

The TiO_2, SiO_2 and SiC presence in the oxidised composite at 750 ℃ is further confirmed by TEM and energy filter mapping (Figs. 8 and 10). This observation is in agreement with all the analysis presented above.

Conclusions

The open cell 3D TiC/SiC composite was oxidised in static air at different temperatures (℃): 350, 450, 550, 650 and 750 under an isothermal regime (3 h) at a heating rate of 3 ℃ min^{-1}. The homogeneous morphology of the inner structure and the excellent dispersion of TiC on SiC in the initial composite may be observed in the SEM and HRTEM images. The TiC particles were in the range from 40 nm to 200 nm and appear to be embedded in the SiC structure. After oxidation, a phase modification can be observed in the composite morphology due to TiO_2 formation. The Raman and XRD analysis showed TiC oxidation starting at 450 ℃ when a mixture of anatase and rutile was observed. By increasing the temperature, a decrease was observed in the anatase mass fraction, indicating the rutile to be more stable than anatase at high temperatures. The TGA and SEM analyses revealed the SiO_2 presence for Ox750, showing that TiC/SiC could be oxidised to TiO_2/SiC up

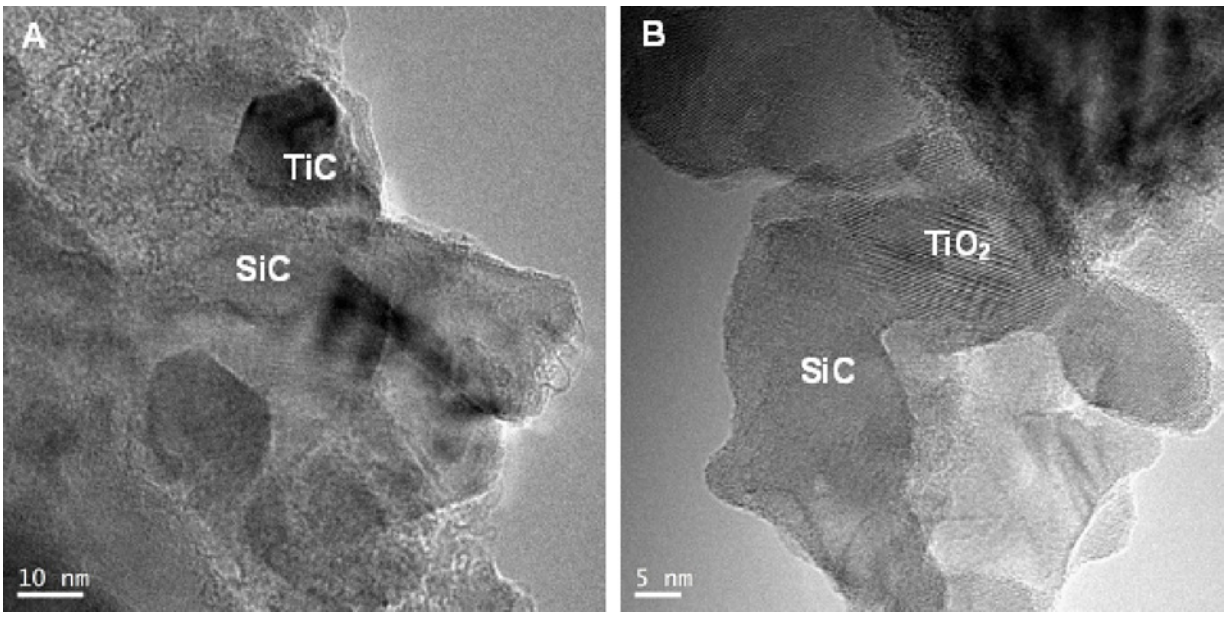

Fig. 8. HRTEM images of raw (A) and Ox750 (B).

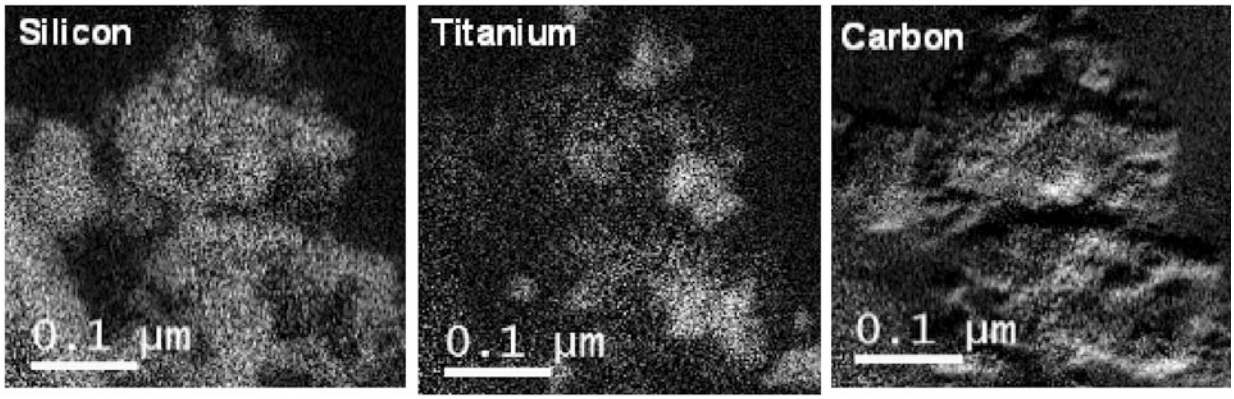

Fig. 9. Energy filter mapping for raw composite.

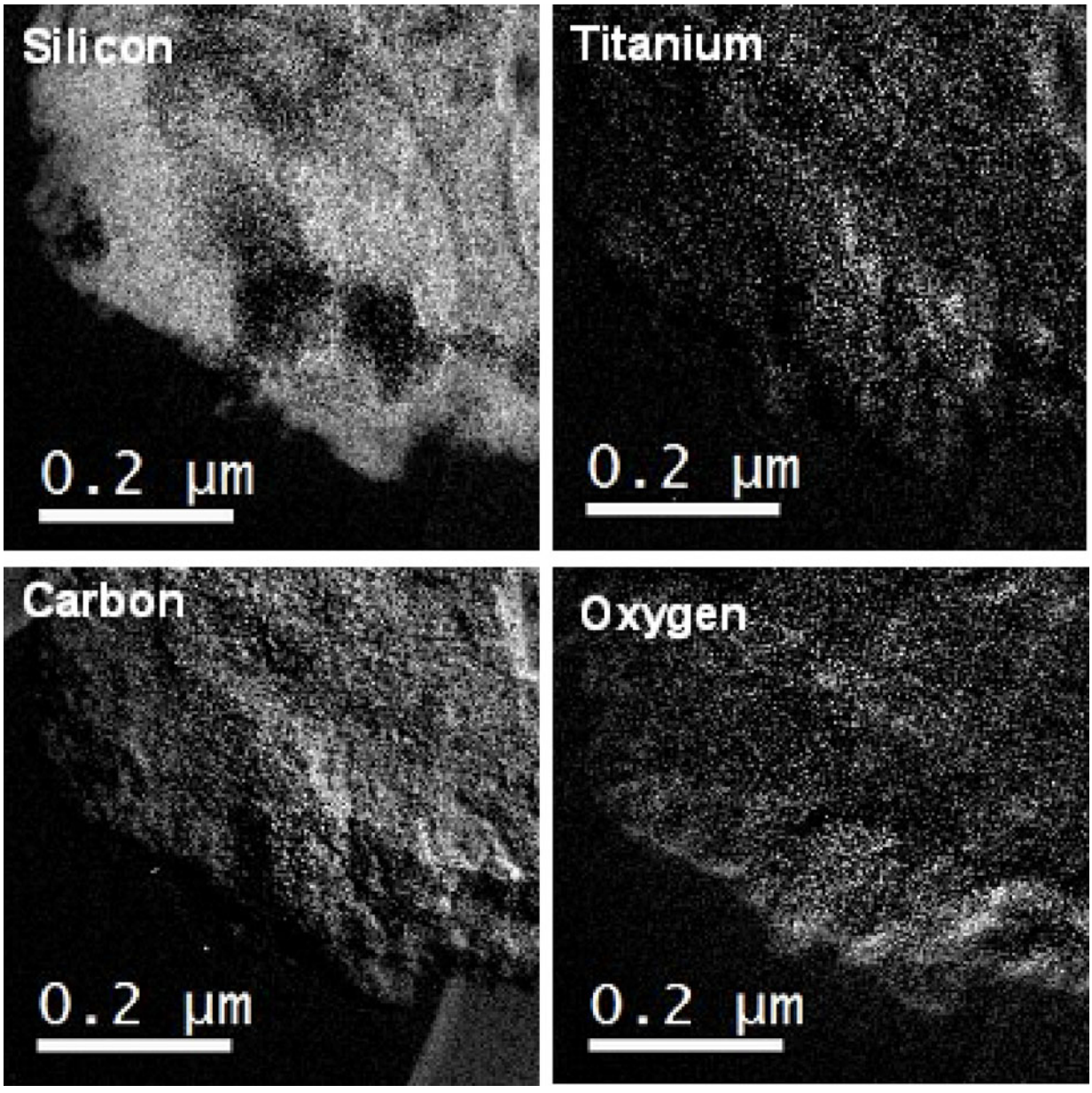

Fig. 10. Energy filter mapping for at Ox750.

to 750 ℃. At higher temperatures, the sample was a $TiO_2/SiO_2/SiC$ mixture. These results can serve as a guideline for catalyst-impregnation/anchoring on rutile, anatase or their mixture.

Acknowledgements. The authors would like to acknowledge the financial support received from the Abu Dhabi Oil Refining Company (TAKREER) and from the Department of Chemical Engineering at The Petroleum Institute, Abu Dhabi, United Arab Emirates.

References

Basile, F., Del Gallo, P., Fornasari, G., Gary, D., Rosetti, V., & Vaccari, A. (2007). SiC as stable high thermal conductive catalyst for enhanced SR process. *Studies in Surface Science and Catalysis*, *167*, 313–318. DOI: 10.1016/s0167-2991(07)80150-9.

de Tymowski, B., Liu, Y. F., Meny, C., Lefèvre, C., Begin, D., Nguyen, P., Pham, C., Edouard, D., Luck, F., & Cuong, P. H. (2012). Co–Ru/SiC impregnated with ethanol as an effective catalyst for the Fischer–Tropsch synthesis. *Applied Catalysis A*, *419*, 31–40. DOI: 10.1016/j.apcata.2012.01.004.

Diebold, U. (2003). The surface science of titanium dioxide. *Surface Science Reports*, *48*, 53–229. DOI: 10.1016/s0167-5729(02)00100-0.

Duran, A., Serna, C., Fornes, V., & Navarro, J. M. F. (1986). Structural considerations about SiO_2 glasses prepared by sol–gel. *Journal of Non-Crystalline Solids*, *82*, 69–77. DOI: 10.1016/0022-3093(86)90112-2.

Fernandez-Torres, L. C., Perry, S. S., Didziulis, S. V., & Frantz, P. P. (2002). The interaction of ammonia with transition metal carbide surfaces. *Surface Science*, *511*, 121–132. DOI: 10.1016/s0039-6028(02)01559-5.

Ghanem, H., Kormann, M., Gerhard, H., & Popovska, N. (2007). Processing of biomorphic porous TiO_2 ceramics by chemical vapor infiltration and reaction (CVI-R) technique. *Journal of the European Ceramic Society*, *27*, 3433–3438. DOI: 10.1016/j.jeurceramsoc.2007.02.197.

Hu, Y., Tsai, H. L., & Huang, C. L. (2003). Effect of brookite phase on the anatase–rutile transition in titania nanoparticles. *Journal of the European Ceramic Society*, *23*, 691–696. DOI: 10.1016/s0955-2219(02)00194-2.

Li, G. B., Zhang, J. Z., Meng, Q. L., & Li, W. Z. (2007). Synthesis of silicon carbide films by combined implantation with sputtering techniques. *Applied Surface Science*, *253*, 8428–8434. DOI: 10.1016/j.apsusc.2007.04.014.

Long, H., Yang, G., Chen, A. P., Li, Y. H., & Lu, P. X. (2008). Growth and characteristics of laser deposited anatase and rutile TiO_2 films on Si substrates. *Thin Solid Films*, *517*, 745–749. DOI: 10.1016/j.tsf.2008.08.179.

Marin, P., Ordonez, S., & Diez, F. V. (2012). Performance of silicon–carbide foams as supports for Pd-based methane combustion catalysts. *Journal of Chemical Technology and Biotechnology*, *87*, 360–367. DOI: 10.1002/jctb.2726.

Martoňák, R., Donadio, D., Oganov, A. R., & Parrinello, M. (2006). Crystal structure transformations in SiO_2 fom classical and ab initio metadynamics. *Nature Materials*, *5*, 623–626. DOI: 10.1038/nmat1696.

Meinhold, G. (2010). Rutile and its applications in earth sciences. *Earth-Science Reviews*, *102*, 1–28. DOI: 10.1016/j.earscirev.2010.06.001.

Merlemejean, T., Abdelmounim, E., & Quintard, P. (1995). Oxide layer on silicon carbide powder: A FT-IR investigation. *Journal of Molecular Structure*, *349*, 105–108. DOI: 10.1016/0022-2860(95)08720-g.

Mirabedini, A., Mirabedini, S. M., Babalou, A. A., & Pazokifard, S. (2011). Synthesis, characterization and enhanced photocatalytic activity of TiO_2/SiO_2 nanocomposite in an aqueous solution and acrylic-based coatings. *Progress in Organic Coatings*, *72*, 453–460. DOI: 10.1016/j.porgcoat.2011.06.002.

Moene, R., Tazelaar, F. W., Makkee, M., & Moulijn, J. A. (1997). Nickel-catalyzed conversion of activated carbon extrudates into high surface area silicon carbide by reactive chemical vapour deposition. *Journal of Catalysis*, *170*, 311–324. DOI: 10.1006/jcat.1997.1782.

Moene, R., Makkee, M., & Moulijn, J. A. (1998). High surface area silicon carbide as catalyst support characterization and stability. *Applied Catalysis A*, *167*, 321–330. DOI: 10.1016/s0926-860x(97)00326-8.

Nguyen, T. V., Lee, H. C., Khan, M. A., & Yang, O. B. (2007). Electrodeposition of TiO_2/SiO_2 nanocomposite for dye-sensitized solar cell. *Solar Energy*, *81*, 529–534. DOI: 10.1016/j.solener.2006.07.008.

Nguyen, P., Nhut, J. M., Edouard, D., Pham, C., Ledoux, M. J., & Pham-Huu, C. (2009). Fe_2O_3/β-SiC: A new high efficient catalyst for the selective oxidation of H_2S into elemental sulfur. *Catalysis Today*, *141*, 397–402. DOI: 10.1016/j.cattod.2008.10.047.

Nguyen, P., & Pham, C. (2011). Innovative porous SiC-based materials: From nanoscopic understandings to tunable carriers serving catalytic needs. *Applied Catalysis A*, *391*, 443–454. DOI: 10.1016/j.apcata.2010.07.054.

Ohsaka, T., Yamaoka, S., & Shimomura, O. (1979). Effect of hydrostatic pressure on the Raman spectrum of anatase (TiO_2). *Solid State Communications*, *30*, 345–347. DOI: 10.1016/0038-1098(79)90648-3.

Okada, K., Yamamoto, N., Kameshima, Y., Yasumori, A., & MacKenzie, K. J. D. (2001). Effect of silica additive on the anatase-to-rutile phase transition. *Journal of the American Ceramic Society*, *84*, 1591–1596. DOI: 10.1111/j.1151-2916.2001.tb00882.x.

Orendorz, A., Brodyanski, A., Losch, J., Bai, L. H., Chen, Z. H., Le, Y. K., Ziegler, C., & Gnaser, H. (2007). Phase transformation and particle growth in nanocrystalline anatase TiO_2 films analyzed by X-ray diffraction and Raman spectroscopy. *Surface Science*, *601*, 4390–4394. DOI: 10.1016/j.susc.2007.04.127.

Raman, V., Bhatia, G., Mishra, A. K., Bhardwaj, S., & Sood, K. N. (2006). Synthesis of silicon carbide nanofibers from pitch blended with sol–gel derived silica. *Materials Letters*, *60*, 3906–3911. DOI: 10.1016/j.matlet.2006.03.138.

Savio, A. K. P. D., Starikov, D., Bensaoula, A., Pillai, R., García, L. L. D., & Hernández, F. C. R. (2012). Tunable TiO_2 (anatase and rutile) materials manufactured by mechanical means. *Ceramics International*, *38*, 3529–3535. DOI: 10.1016/j.ceramint.2011.12.067.

Schmirler, M., Glenk, F., & Etzold, B. J. M. (2011). In-situ thermal activation of carbide-derived carbon. *Carbon*, *49*, 3679–3686. DOI: 10.1016/j.carbon.2011.05.003.

Schwan, J., Ulrich, S., Batori, V., Ehrhardt, H., & Silva, S. R. P. (1996). Raman spectroscopy on amorphous carbon films. *Journal of Applied Physics*, *80*, 440–447. DOI: 10.1063/1.362745.

Shimada, S. (1996). A thermoanalytical study of oxidation of TiC by simultaneous TGA-DTA-MS analysis. *Journal of Materials Science*, *31*, 673–677. DOI: 10.1007/bf00367884.

Sreekantan, S., Hazan, R., & Lockman, Z. (2009). Photoactivity of anatase-rutile TiO_2 nanotubes formed by anodization method. *Thin Solid Films*, *518*, 16–21. DOI: 10.1016/j.tsf.2009.06.002.

van der Meulen, T., Mattson, A., & Osterlund, L. (2007). A comparative study of the photocatalytic oxidation of

propane on anatase, rutile and mixed-phase anatase–rutile TiO_2 nanoparticles: Role of surface intermediates. *Journal of Catalysis*, *251*, 131–144. DOI: 10.1016/j.jcat.2007.07.002.

Wang, Q., Sun, W. Z., Jin, G. Q., Wang, Y. Y., & Guo, X. Y. (2008). Biomorphic SiC pellets as catalyst support for partial oxidation of methane to syngas. *Applied Catalysis B*, *79*, 307–312. DOI: 10.1016/j.apcatb.2007.10.032.

Worch, M., Engelmann, H. J., Blum, W., & Zschech, E. (2002). Cross-sectional thin film characterization of Si compounds in semiconductor device structures using both elemental and ELNES mapping by EFTEM. *Thin Solid Films*, *405*, 198–204. DOI: 10.1016/s0040-6090(01)01680-7.

Xia, Y. D., Yang, Z. X., & Zhu, Y. Q. (2013). Porous carbon-based materials for hydrogen storage: Advancement and challenges. *Journal of Materials Chemistry A*, *1*, 9365–9381. DOI: 10.1039/c3ta10583k.

Yoshikawa, M., Iwagami, K., Morita, N., Matsunobe, T., & Ishida, H. (1997). Characterization of fluorine-doped silicon dioxide film by Raman spectroscopy. *Thin Solid Films*, *310*, 167–170. DOI: 10.1016/s0040-6090(97)00393-3.

Zhang, L. H., & Koka, R. V. (1998). A study on the oxidation and carbon diffusion of TiC in alumina–titanium carbide ceramics using XPS and Raman spectroscopy. *Materials Chemistry and Physics*, *57*, 23–32. DOI: 10.1016/s0254-0584(98)00187-4.